The effect of non-stoichiometry on the hydrogen storage properties of Ti-substituted AB_2 alloys

2003 J. Phys.: Condens. Matter 15 7501

(http://iopscience.iop.org/0953-8984/15/44/006)

INSTITUTE OF PHYSICS PUBLISHING JOURNAL OF PHYSICS: CONDENSED MATTER

J. Phys.: Condens. Matter **15** (2003) 7501–7517 PII: S0953-8984(03)65371-3

The effect of non-stoichiometry on the hydrogen storage properties of Ti-substituted AB_2 alloys

M Kandavel and S Ramaprabhu[1]

Alternate Energy Technology and Magnetic Materials Laboratory, Department of Physics, Indian Institute of Technology Madras, Chennai-600 036, India

E-mail: ramp@iitm.ac.in

Received 26 June 2003
Published 24 October 2003
Online at stacks.iop.org/JPhysCM/15/7501

Abstract

Pressure–composition isotherms have been obtained for $Ti_{0.1}Zr_{0.9}Mn_{0.9}V_{0.1}Fe_{0.5}Ni_{0.5}$, $(Ti_{0.1}Zr_{0.9})_{1.1}Mn_{0.9}V_{0.1}Fe_{0.5}Ni_{0.5}$, $Ti_{0.1}Zr_{0.9}(Mn_{0.9}V_{0.1})_{1.1}Fe_{0.5}Ni_{0.5}$ and $Ti_{0.1}Zr_{0.9}Mn_{0.9}V_{0.1}Fe_{0.55}Ni_{0.55}$ having the C14 type hexagonal structure in the temperature and pressure ranges 30–100 °C and 0.1–50 bar using a pressure reduction method in order to find the effect of non-stoichiometry on hydrogen storage properties. The powder x-ray diffractograms of the alloys show the formation of C14 single phase; the lattice constants and unit cell volumes of these alloys have been calculated. $Ti_{0.1}Zr_{0.9}(Mn_{0.9}V_{0.1})_{1.1}Fe_{0.5}Ni_{0.5}$ has a hydrogen storage capacity of 3.5 hydrogen atoms/fu at 20 bar and room temperature. The dependences of the thermodynamics of the dissolved hydrogen in these alloy hydrides in the temperature range 30–100 °C on the hydrogen concentration have shown the existence of α, $\alpha + \beta$ and β phase regions as seen in the isotherms. The effect of non-stoichiometry on the kinetics of hydrogen absorption in these alloys has been studied at 50 °C. The powder x-ray diffractograms of the alloy hydrides show that these alloys do not undergo any structural change upon hydrogenation and that there is only a volume expansion of around 25%. The activation energy and diffusion coefficient of dissolved hydrogen in $Ti_{0.1}Zr_{0.9}Mn_{0.9}V_{0.1}Fe_{0.5}Ni_{0.5}$ have been calculated from the kinetics of hydrogen absorption measurements at different temperatures. The activation energy is $E_a = 0.17$ eV in the $\alpha + \beta$ phase region and $E_a = 0.22$ eV in the β phase region and the diffusion coefficient $D = 2.7 \times 10^{-11}$ cm^2 s^{-1} in the β phase at 30 °C.

1. Introduction

Metal hydrides have acquired considerable scientific and technological significance in recent years [1, 2]. The dramatic changes observed in the electronic and magnetic properties of

[1] Author to whom any correspondence should be addressed.

the host metal on hydrogenation have been challenging to scientists. The remarkably large hydrogen storage capacity of the hydrides at ambient temperature and favourable hydrogen pressure have attracted technological interest as regards a variety of engineering applications such as hydrogen storage, heat pumping and refrigeration. The $LaNi_5$ and TiFe types of compound have been studied to a great extent as hydrogen storage materials [3, 4]. However, their heavy weight, high cost and endothermic hydrogenation nature have led to searches for better hydrogen storage materials. The AB_2 Laves phases are a class of alloys that are considered to be promising candidates for providing hydrogen storage material and negative electrodes for Ni–MH batteries. Laves phases are intermetallic compounds typified by three prototype crystal structures: hexagonal C14 ($MgZn_2$ type), cubic C15 ($MgCu_2$ type) and hexagonal C36 ($MgNi_2$ type) [5]. Recently, interest in the study of Zr-based AB_2 type Laves phase intermetallic compounds has increased because of their high hydrogen storage capacity. The stoichiometric Zr-based AB_2 compound can be stabilized either as C14 or C15 type and absorbs around 3.4 hydrogen atoms/fu at room temperature [6, 7].

The activation states of the alloys play fundamental roles in the absorption process, since they define the rates of reaction of the hydrogen with the metal. During activation [8–10], different processes can occur such as (1) reduction of metal surface oxides that interfere with hydrogen, (2) reduction in particle size due to cracks produced by the increase in volume, (3) changes in the chemical composition and/or in the surface structure of the metal. In efforts to improve the initial activation process, extensive studies have been carried out with reference to the composition of the alloy and to an anodic oxidation treatment. High discharge capacities [11, 12] (350–400 mA h g^{-1}) were reported for Zr-based over-stoichiometric AB_2 alloys with low Ti content at discharge currents of up to 220 mA g^{-1} without cycle life tests.

Our earlier study on the systems $ZrMnFe_{1-x}Ni_x$ and $ZrMnFe_{1-x}Co_x$ [13, 14] ($x = 0.2$, 0.4, 0.5 and 0.6) revealed that the slope of hydrogen absorption plateau is small for $ZrMnFe_{0.5}Ni_{0.5}$ and $ZrMnFe_{0.5}Co_{0.5}$ as compared to those of the other alloys due to increase in the degree of order caused by the presence of Fe and Ni/Co in a 1:1 mole ratio. In the present study, we have chosen alloys with Fe and Ni in a 1:1 mole ratio and we have studied the influence on the hydrogen storage properties of substitutions of Ti and V at Zr and Mn sites respectively. As a second step, we analysed the hydrogen storage properties of the over-stoichiometric alloys at A, B_1 and B_2 sites in the AB_2 alloy. We present here the hydrogen storage properties of $Ti_{0.1}Zr_{0.9}Mn_{0.9}V_{0.1}Fe_{0.5}Ni_{0.5}$ and the over-stoichiometric alloys $(Ti_{0.1}Zr_{0.9})_{1.1}Mn_{0.9}V_{0.1}Fe_{0.5}Ni_{0.5}Ti_{0.1}Zr_{0.9}(Mn_{0.9}V_{0.1})_{1.1}Fe_{0.5}Ni_{0.5}$ and $Ti_{0.1}Zr_{0.9}Mn_{0.9}V_{0.1}Fe_{0.55}Ni_{0.55}$ in the ranges 30–100 °C and 0.1–50 bar and the effects of non-stoichiometry on their hydrogen storage properties are discussed.

2. Experimental details

Alloys have been prepared in an arc furnace under an argon atmosphere of about 0.80 bar with stoichiometric proportions of high purity constituent elements, with 6 wt% of excess Mn added to the total mixture following the normal procedure, since the vapour pressure of Mn is very high. The alloy buttons were then remelted six times, turning them upside down to ensure homogeneity. The weight loss percentage of these samples during these preparations was less than 0.2%. In order to identify the crystal structure and to obtain the lattice parameters of these alloys, x-ray diffraction analysis using Fe Kα radiation was carried out using Si as a standard reference. Since as formed alloys showed single phase formation, no further annealing treatment was given.

Pressure–composition–temperature (P–C–T) isotherms were obtained for the temperature range 30–100 °C and the pressure range 0.1–50 bar using a conventional gasometric

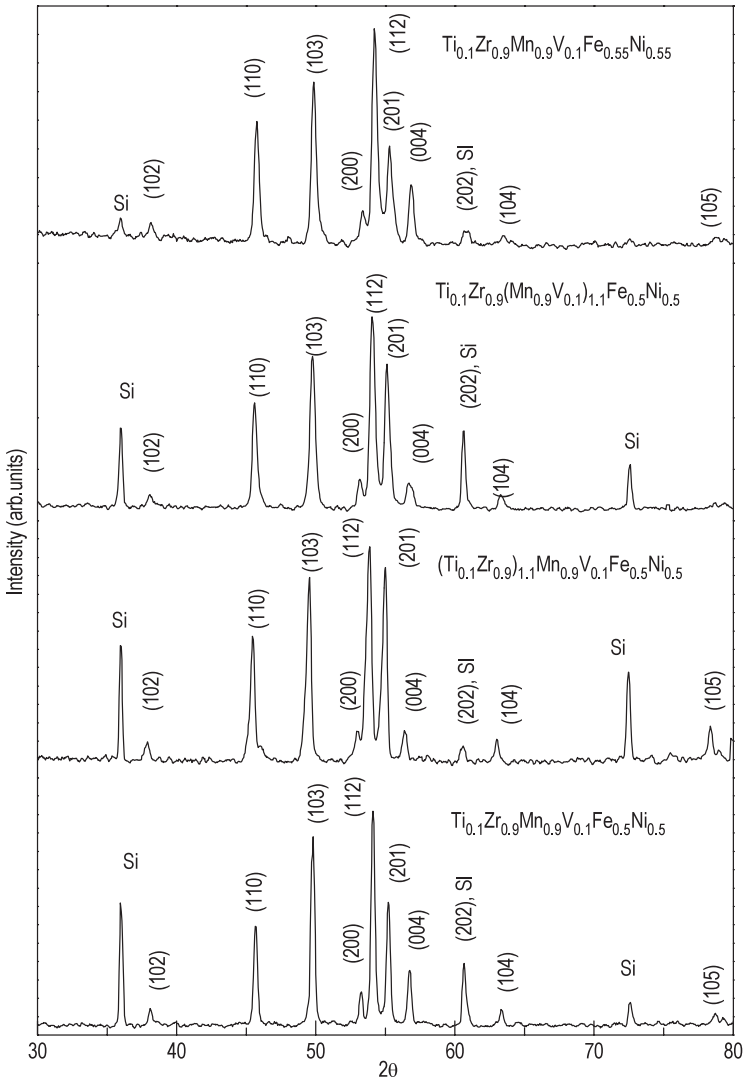

Figure 1. Powder x-ray diffractograms of the alloys obtained with Fe Kα radiation.

technique [15]. Hydrogen absorption pressure–composition isotherms and kinetics data were collected by a conventional gasometric technique. An apparatus based on the pressure reduction method and operating in the temperature range 30–300 °C and in the pressure range 0.1–100 bar was employed. About 0.5 g of the pulverized powder sample was introduced into the high pressure reactor and evacuated to 10^{-6} Torr. For activation purposes, alloy powder was exposed to a hydrogen atmosphere at a pressure of 20 bar. From the reduction of the hydrogen pressure, the amount of hydrogen absorbed by the sample was calculated. Dehydriding was performed by evacuating and then heating the hydride powder at 200 °C for 3 h. After three such cycles of hydriding and dehydriding, the amount of hydrogen absorbed by the sample remained the same. After the activation process, absorption P–C–T data were collected. Following each experiment, the sample was degassed at 200 °C under a vacuum of 10^{-6} Torr. The kinetics data were collected by recording the change in pressure as a function of time at constant temperature.

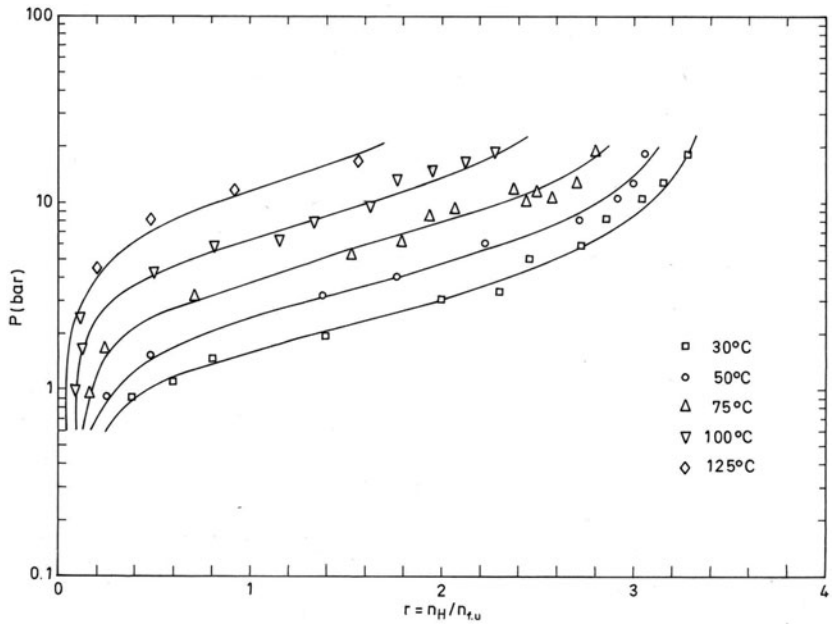

Figure 2. Hydrogen absorption isotherms of $Ti_{0.1}Zr_{0.9}Mn_{0.9}V_{0.1}Fe_{0.5}Ni_{0.5}$.

Table 1. The lattice parameters, unit cell volume and ANOE for the alloys. (Note: the values of a and c are given with accuracies of 0.001 and 0.001 Å respectively. The values of the unit cell volume are given with an accuracy of 0.1 $Å^3$.)

Alloy	a (Å)	c (Å)	v ($Å^3$)	ANOE
$Ti_{0.1}Zr_{0.9}Mn_{0.9}V_{0.1}Fe_{0.5}Ni_{0.5}$	4.993	8.152	176.0	6.60
$(Ti_{0.1}Zr_{0.9})_{1.1}Mn_{0.9}V_{0.1}Fe_{0.5}Ni_{0.5}$	5.014	8.200	178.5	6.73
$Ti_{0.1}Zr_{0.9}(Mn_{0.9}V_{0.1})_{1.1}Fe_{0.5}Ni_{0.5}$	5.000	8.159	176.7	6.82
$Ti_{0.1}Zr_{0.9}Mn_{0.9}V_{0.1}Fe_{0.55}Ni_{0.55}$	4.984	8.142	175.2	6.90

3. Results and discussion

3.1. Crystal structure

The room temperature Fe Kα powder x-ray diffraction patterns confirmed the single phase nature of these systems which crystallize in the C14 structure with space group $P6_3/mmc$ (figure 1). Since the changes in the lattice parameters were very small, the lattice parameters were obtained more precisely by using Si as the standard by mixing Si with the alloys while taking the diffractograms. The average number of outer electrons (ANOE) in these alloys is less than seven indicating a preference for the formation of the C14 structure [16]. The lattice parameters and unit cell volume were evaluated using a least squares refinement technique and are listed in table 1.

The cell parameters of the non-stoichiometric alloys differ from those of the stoichiometric alloy due to the increase in the atomic proportions of the corresponding elements at non-stoichiometric positions. The lattice constants and unit cell volumes of these alloys decrease as the position of the non-stoichiometry moves from A to B_2 sites.

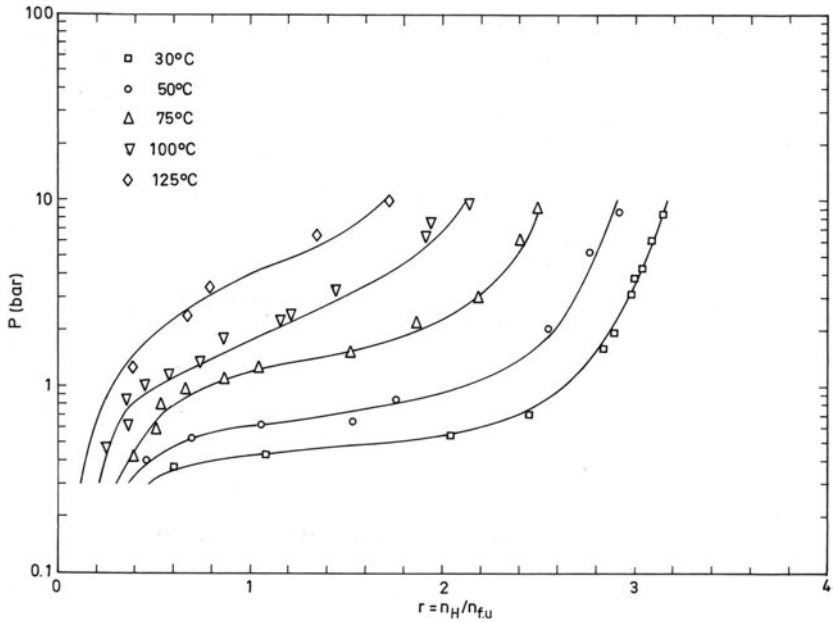

Figure 3. Hydrogen absorption isotherms of $(Ti_{0.1}Zr_{0.9})_{1.1}Mn_{0.9}V_{0.1}Fe_{0.5}Ni_{0.5}$.

3.2. P–C isotherms

The hydrogen absorption isotherms have been studied for these alloys in the temperature and pressure ranges 30–100 °C and 0.1–50 bar and they are shown in figures 2–5. These hydrogen absorption isotherms have indicated that there are two single phase regions (α, β) and one two phase region ($\alpha + \beta$) in the temperature and pressure ranges studied. The maximum storage capacity of the non-stoichiometric alloys has been shown to be higher than that of the stoichiometric alloy, since excess amounts in atomic proportions of the elements interact with hydrogen in a non-stoichiometric alloy as compared to the corresponding stoichiometric alloy. The maximum storage capacity was found to be around 3.5 hydrogen atoms/fu at 20 bar and 30 °C in $Ti_{0.1}Zr_{0.9}(Mn_{0.9}V_{0.1})_{1.1}Fe_{0.5}Ni_{0.5}$. The plateau pressure of the hydrogen storage alloy strongly depends on both the unit cell volume of the alloy and the electronic structure of the alloy. At any particular temperature, the plateau pressure of these alloys increases with the position of the over-stoichiometry: at A, B_1 and B_2 sites, which is due to the contraction of the unit cell volume and the interstitial hole size. This causes an increase in strain energy in order to accommodate the dissolved hydrogen atoms in the interstitial sites. Figure 6 gives the dependence of the plateau pressure at 30 and 50 °C on the unit cell volume for these alloys.

The relative partial molar enthalpy (ΔH_H) and relative partial molar entropy (ΔS_H) of the dissolved hydrogen in these alloy hydrides can be obtained at any particular concentration of hydrogen from the Van't Hoff equation [17],

$$\ln P_{H_2} = 2\left(\frac{\Delta H_H}{RT} - \frac{\Delta S_H}{R}\right). \tag{1}$$

Values of ΔH_H and ΔS_H for dissolved hydrogen for a particular r value have been obtained by a least squares technique from the slope and intercept of $\ln P_{H_2}$ and $1/T$ plots, respectively, and values of ΔH_H for $Ti_{0.1}Zr_{0.9}Mn_{0.9}V_{0.1}Fe_{0.5}Ni_{0.5}$–H, $(Ti_{0.1}Zr_{0.9})_{1.1}Mn_{0.9}V_{0.1}Fe_{0.5}Ni_{0.5}$–H, $Ti_{0.1}Zr_{0.9}(Mn_{0.9}V_{0.1})_{1.1}Fe_{0.5}Ni_{0.5}$–H and $Ti_{0.1}Zr_{0.9}Mn_{0.9}V_{0.1}Fe_{0.55}Ni_{0.55}$–H are plotted as a

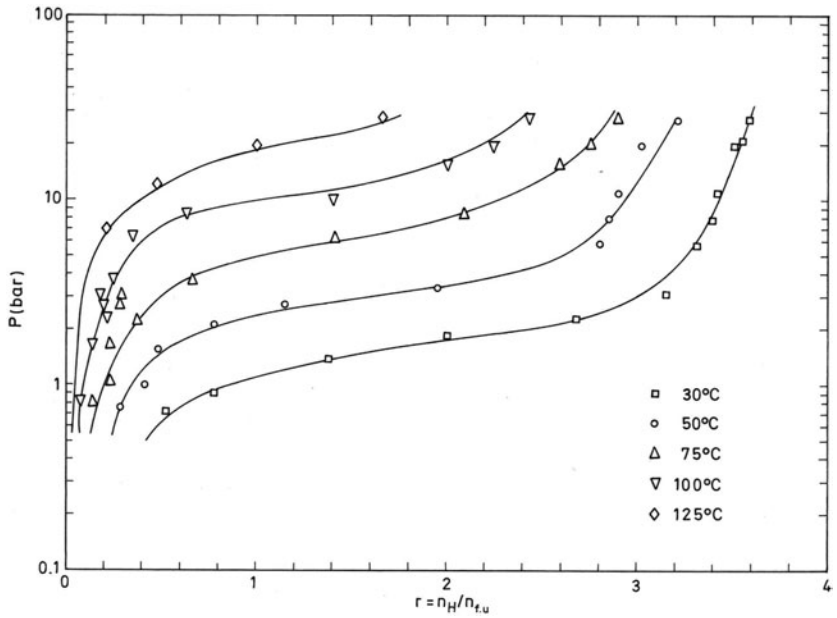

Figure 4. Hydrogen absorption isotherms of $Ti_{0.1}Zr_{0.9}(Mn_{0.9}V_{0.1})_{1.1}Fe_{0.5}Ni_{0.5}$.

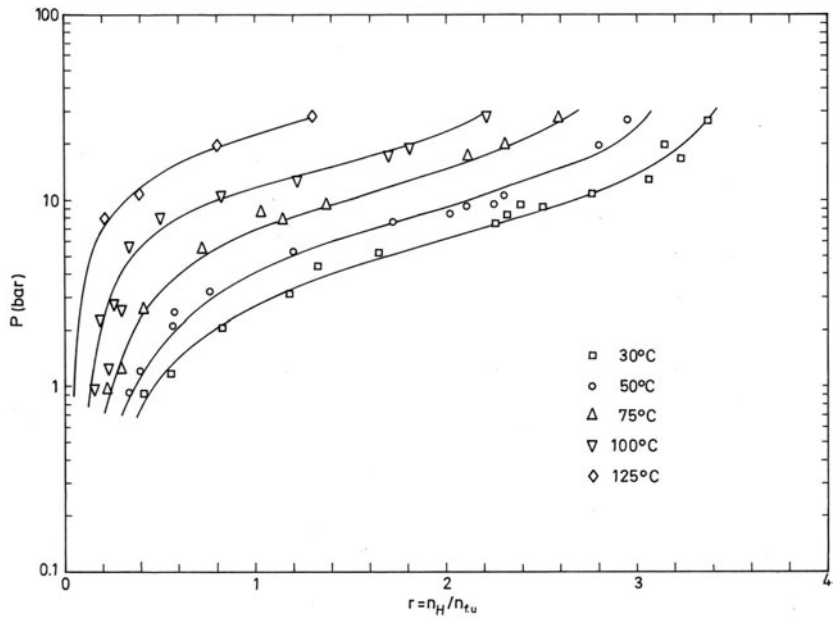

Figure 5. Hydrogen absorption isotherms of $Ti_{0.1}Zr_{0.9}Mn_{0.9}V_{0.1}Fe_{0.55}Ni_{0.55}$.

function of hydrogen concentration (figure 7). Since the heat of formation differs for the different phases, its variation with hydrogen concentration gives different slopes for different phase regions, α, $\alpha + \beta$ and β, in the system. These phase regions and phase region boundaries agree well with those observed in the P–C isotherms. The Gibbs free energies

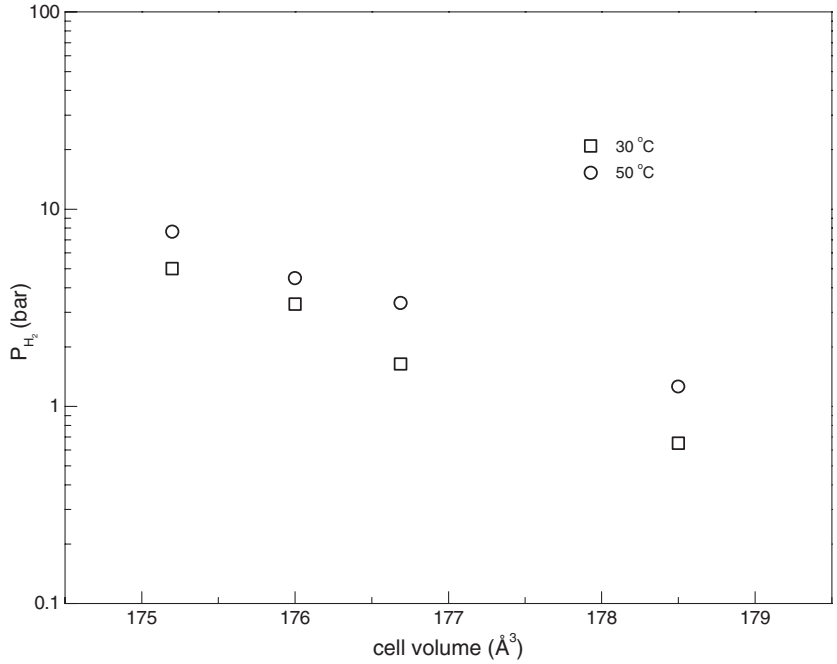

Figure 6. The variation of plateau pressure with unit cell volume for the alloys.

Table 2. The equilibrium pressure, plateau slope, ΔH_H, ΔS_H and $\Delta \mu_H$ for these alloy hydrides.

Alloy hydrides	Plateau pressure[a] 30 °C, 50 °C	Plateau slope[b]	$-\Delta H_H$ (kJ/mol H)	$-\Delta S_H$ (J K^{-1}/mol H)	$\Delta \mu_H$ (kJ/mol H) 30 °C, 50 °C
$Ti_{0.1}Zr_{0.9}Mn_{0.9}V_{0.1}Fe_{0.5}Ni_{0.5}$–H	2.4, 3.7	2.2	9.7	35.7	1.1, 1.8
$(Ti_{0.1}Zr_{0.9})_{1.1}Mn_{0.9}V_{0.1}Fe_{0.5}Ni_{0.5}$–H	0.4, 0.8	2.5	13.4	40.8	−1.0, −0.2
$Ti_{0.1}Zr_{0.9}(Mn_{0.9}V_{0.1})_{1.1}Fe_{0.5}Ni_{0.5}$–H	1.5, 3.1	1.4	14.1	48.4	0.5, 1.5
$Ti_{0.1}Zr_{0.9}Mn_{0.9}V_{0.1}Fe_{0.55}Ni_{0.55}$–H	4.6, 6.9	2.8	8.7	35.1	1.9, 2.6

[a] Plateau pressure at $r = n_H/n_{fu} = 1.6$.
[b] $\ln(P_{H/fu=3.0}/P_{H/fu=0.4})$.

($\Delta \mu_H = \Delta H_H - T\,\Delta S_H$) at 30 and 50 °C, along with ΔH_H and ΔS_H, are listed in table 2. The dependence of $\Delta \mu_H$ on the unit cell volume for the alloys (tables 1 and 2) suggests that the strain energy required to accommodate the interstitial hydrogen decreases with increase in size of these interstitial sites, in keeping with the increase in unit cell volume of these alloys.

3.3. Kinetics of hydrogen absorption

In the present study, the kinetics of hydrogen absorption was studied using a Sievert's apparatus, for measuring the hydrogen pressure change due to hydrogen absorption in a closed system of constant volume. Figure 8 shows a typical measurement of the kinetics of hydrogen absorption of $Ti_{0.1}Zr_{0.9}Mn_{0.9}V_{0.1}Fe_{0.5}Ni_{0.5}$ at different temperatures. One can expect, from the rates of hydrogen absorption, the three different phase regions (α, $\alpha + \beta$ and β) in the kinetics measurement, as seen in the P–C isotherms [18]. But in the present study, the α phase stage

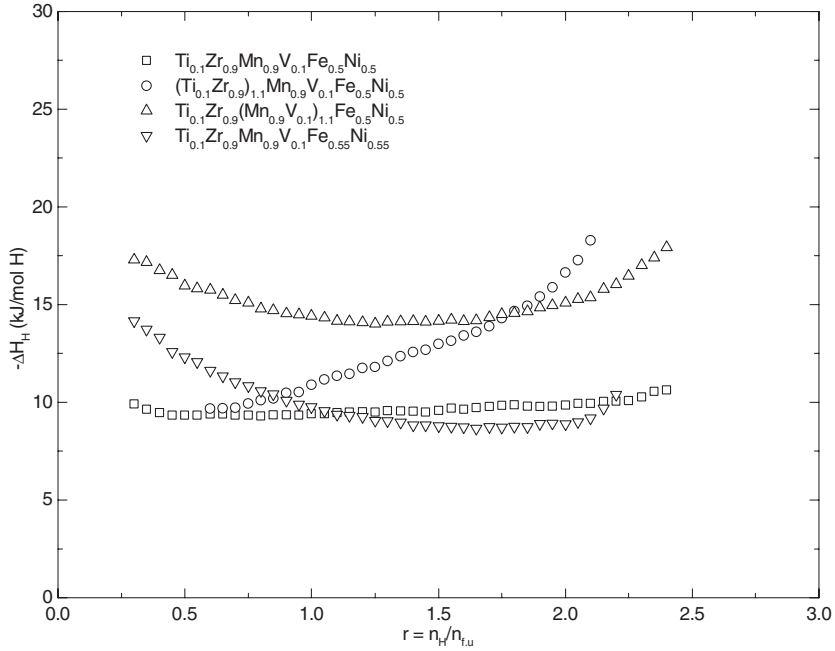

Figure 7. The variation of ΔH_{H} with hydrogen concentration in these alloy hydrides.

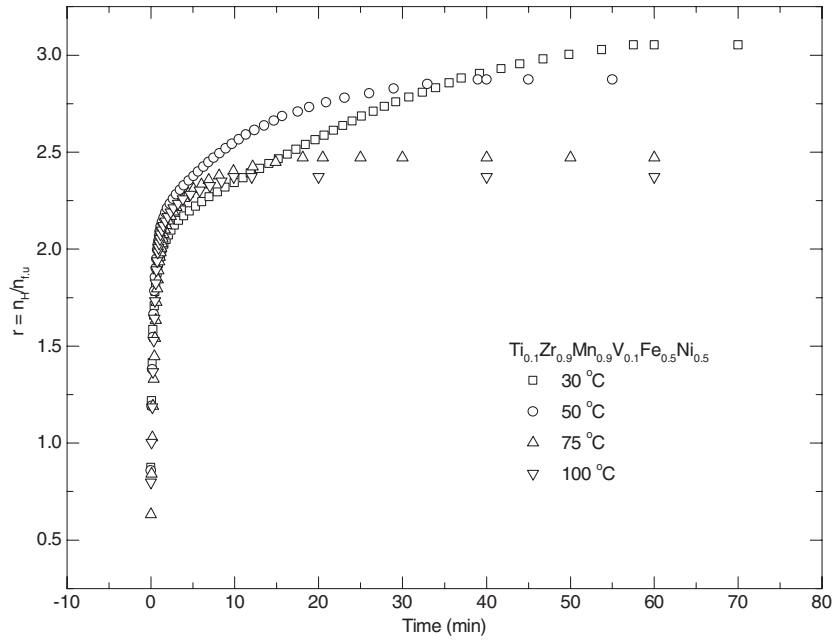

Figure 8. The hydrogen absorption kinetics of $Ti_{0.1}Zr_{0.9}Mn_{0.9}V_{0.1}Fe_{0.5}Ni_{0.5}$ at different temperatures.

was not observed due to the fast reaction rate, while two different reaction rates corresponding to $\alpha + \beta$ and β phases were observed with our experimental conditions. The absorption rate is

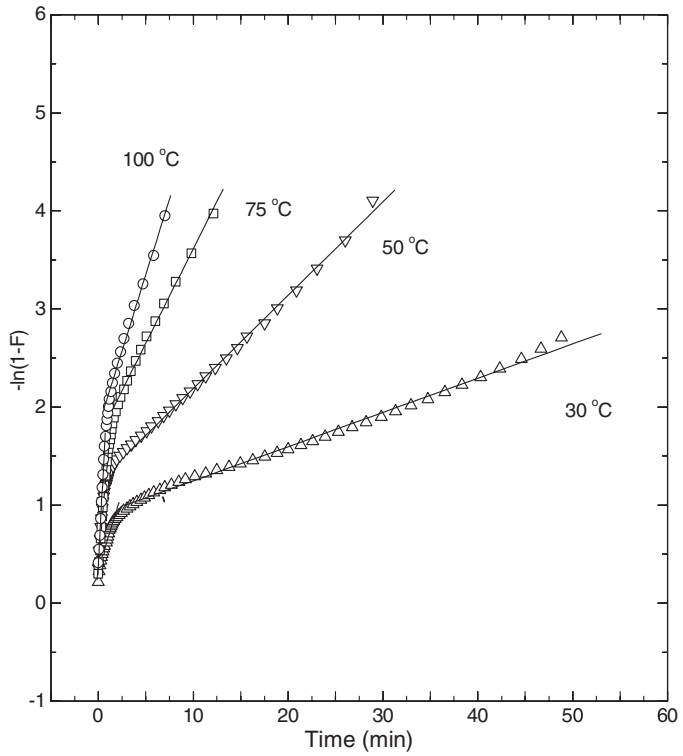

Figure 9. $-\ln(1-F)$ versus t plots for $Ti_{0.1}Zr_{0.9}Mn_{0.9}V_{0.1}Fe_{0.5}Ni_{0.5}$–H at different temperatures.

given by Lee *et al* [19]:

$$\frac{dm}{dt} = k(P - P_c). \tag{2}$$

Most of the hydrogen diffusion and the $\alpha \rightarrow \beta$ phase transformation reaction mechanisms in metals are of first order [19]. Therefore the rate is given by

$$\frac{dC}{dt} = kC^n \tag{3}$$

where C is the hydrogen concentration in the gas phase; k is the reaction constant at constant temperature and $n = 1$.

Therefore,

$$-\ln\frac{C}{C_0} = kt \tag{4}$$

where $C = C_0$ at $t = 0$. If C is replaced by the hydrogen content m in the solid state ($C_0 = m_\infty - m_0$ and $C = m_\infty - m$ where m_∞ and m_0 are the values of m at $t = \infty$ and 0 respectively),

$$-\ln\left(1 - \frac{m - m_0}{m_\infty - m_0}\right) = -\ln(1 - F) = kt \tag{5}$$

where F is the equilibrium rate which is m/m_∞ for $m_0 = 0$ at $t = 0$.

To obtain reaction constants k using equation (5), the results of the hydrogen absorption process for various constant temperatures and pressures are plotted as $-\ln(1 - F)$ versus t.

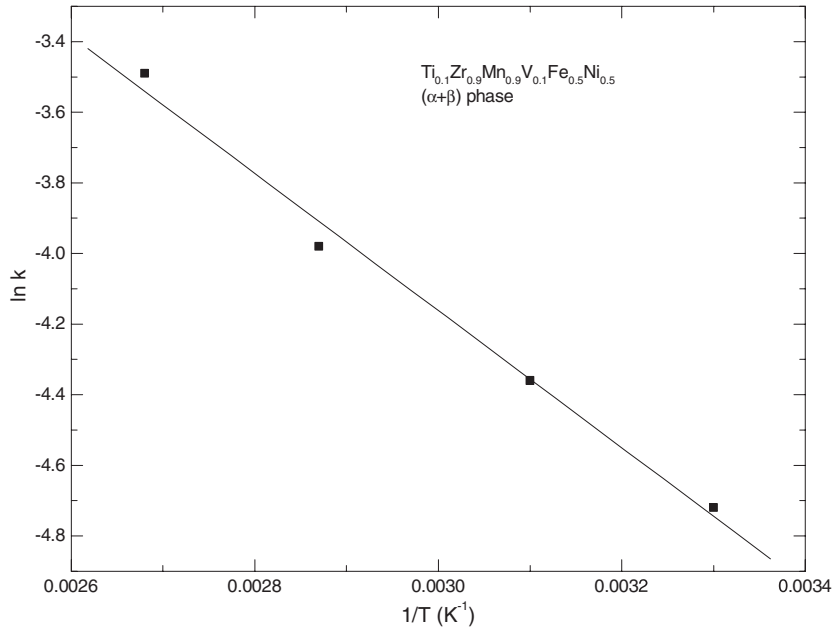

Figure 10. A $\ln k$ versus $1/T$ plot in the $\alpha + \beta$ phase for $Ti_{0.1}Zr_{0.9}Mn_{0.9}V_{0.1}Fe_{0.5}Ni_{0.5}$–H.

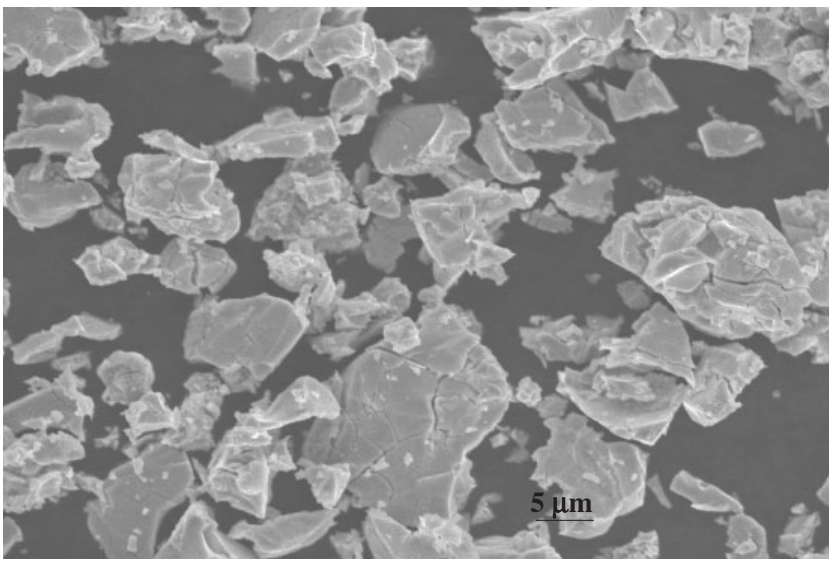

Figure 11. A typical SEM image of $Ti_{0.1}Zr_{0.9}Mn_{0.9}V_{0.1}Fe_{0.5}Ni_{0.5}$–H.

It may be seen from figure 9 that the experimental data fit to two linear segments and a gradual slope change occurs. This implies that two different processes are controlling the rate at the initial and final stages of the absorption reaction. It was found from the P–C isotherms that the concentration at which the slope changes corresponds to the region of the $\alpha + \beta$ phase to β phase transition [20]. The first linear segment would seem to correspond to the $\alpha + \beta$ phase and the second one to the β phase.

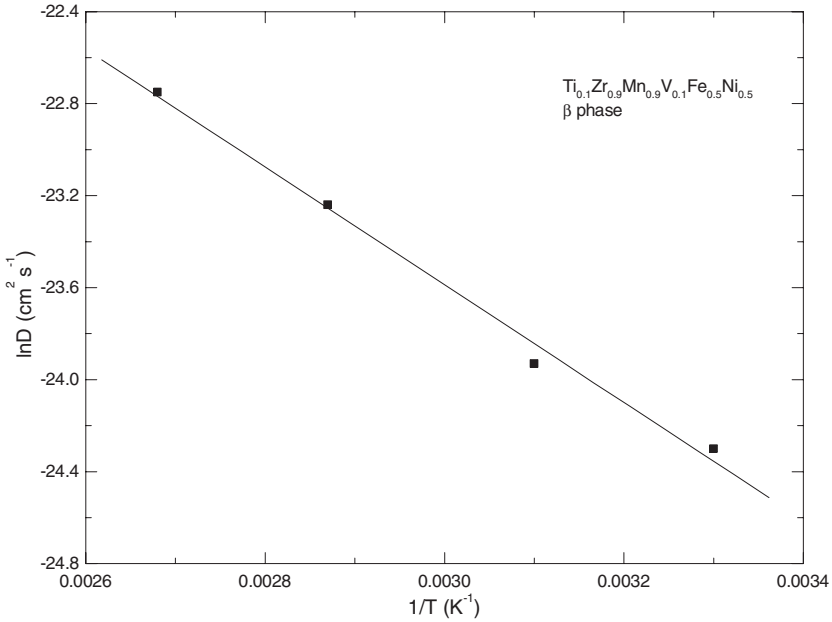

Figure 12. A ln D versus $1/T$ plot in the β phase for $Ti_{0.1}Zr_{0.9}Mn_{0.9}V_{0.1}Fe_{0.5}Ni_{0.5}$–H.

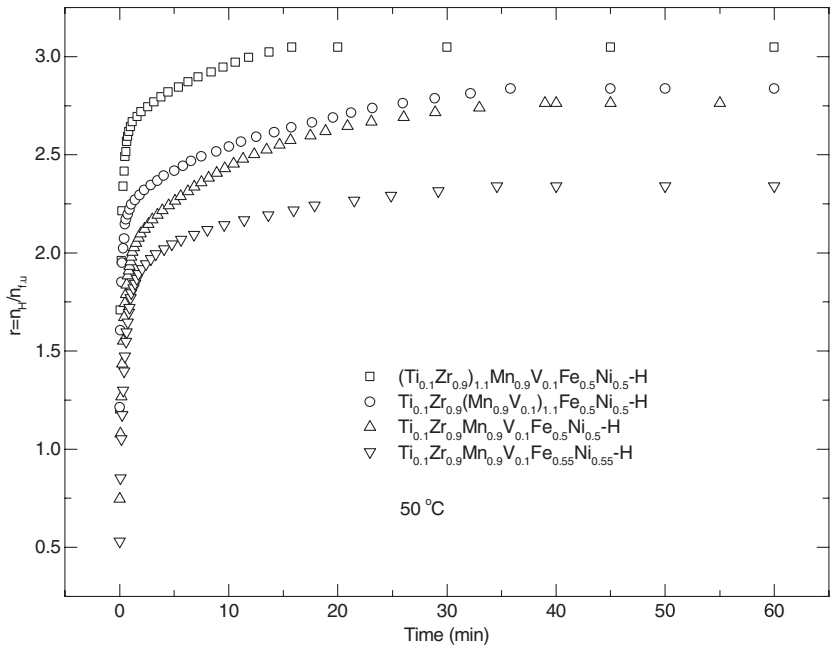

Figure 13. The hydrogen absorption kinetics of these alloys at 50 °C.

It would appear that the absorption rate is controlled by different mechanisms when the reactions proceed through different phase regions. The possible rate determining steps involved in the hydrogen absorption kinetics are the surface process, the interface process and

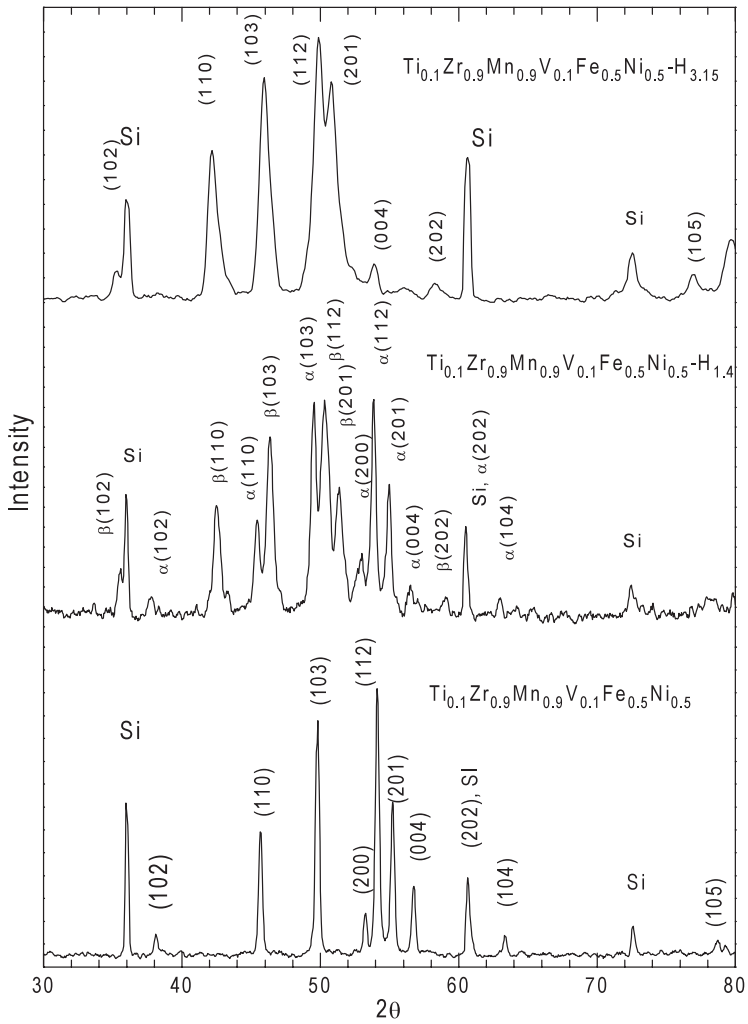

Figure 14. Powder x-ray diffractograms of $Ti_{0.1}Zr_{0.9}Mn_{0.9}V_{0.1}Fe_{0.5}Ni_{0.5}$–H.

the diffusion. The surface process, chemisorption and nucleation of the hydrides occur at the initial stage of absorption; these seem to go unnoticed in our case, because of the fast reaction kinetics in the α phase.

As the absorption process proceeds further, the hydride phase nuclei start growing. After some time, the growing hydride phase nuclei contact with each other, with a corresponding decrease in interfacial area, and in this process the reaction rate is controlled by the phase transformation at the $\alpha \rightarrow \beta$ interface [21]. This stage may be the process related to the first linear segment of the fit shown in figure 9 corresponding to the $\alpha + \beta$ phase region. The rate constants k have been calculated for the $\alpha + \beta$ phase, corresponding to the interface process, at various temperature from the slope of the first linear region of the fit shown in figure 9. The activation energy E_a can be calculated from the temperature dependence of the rate constant

$$k = k_0 \exp\left(-\frac{E_a}{k_B T}\right). \tag{6}$$

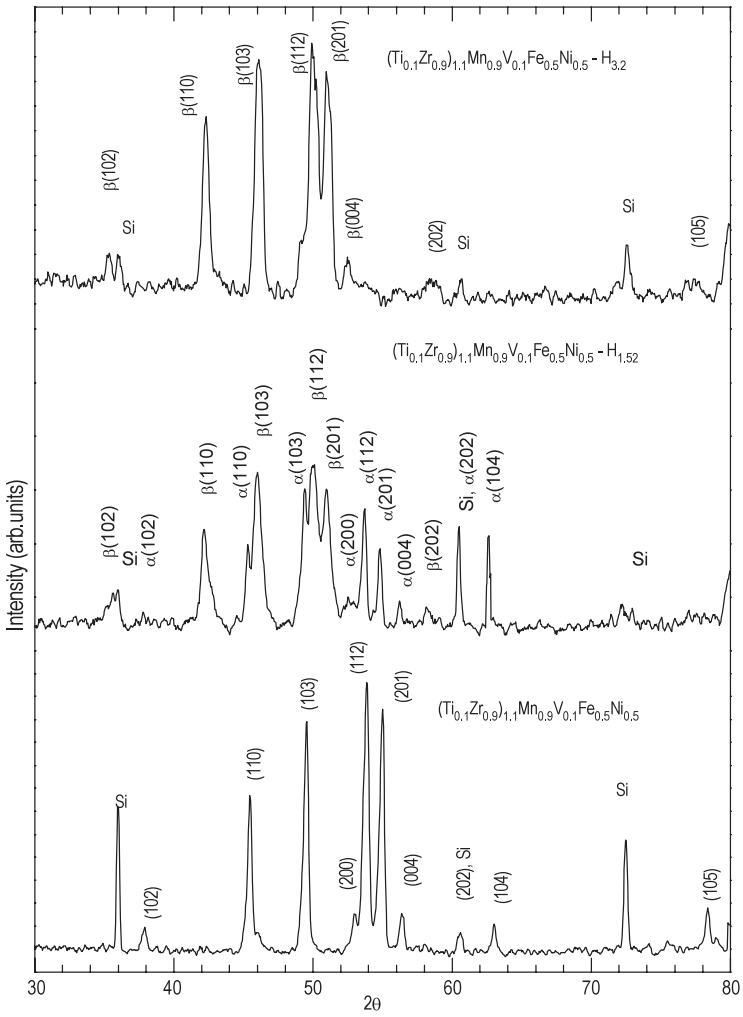

Figure 15. Powder x-ray diffractograms of $(Ti_{0.1}Zr_{0.9})_{1.1}Mn_{0.9}V_{0.1}Fe_{0.5}Ni_{0.5}$–H.

Figure 10 shows an Arrhenius plot of $\ln k$ versus $1/T$ for the interface process. A related activation energy E_a and corresponding frequency factor k_0 were obtained from the slope and Y intercept; the values of E_a and k_0 from these measurements are 0.17 eV and 0.034 s^{-1} respectively.

When the β phase hydride is formed completely, the diffusion of hydrogen should constitute the rate determining step [22, 23] and therefore this may be the case for the second linear region of the fit shown in figure 9, which corresponds to the β phase. The appropriate rate constants have been calculated for the β phase region corresponding to the diffusion process, at various temperatures, from the slope of the straight line. It was then possible to determine the diffusion coefficient (D) from the rate constant of the diffusion controlled reaction.

A value of the hydrogen diffusion coefficient can also be obtained for the hydrogen content m_t at time t for spherical particles with radius r, from the first term of the series expansion of

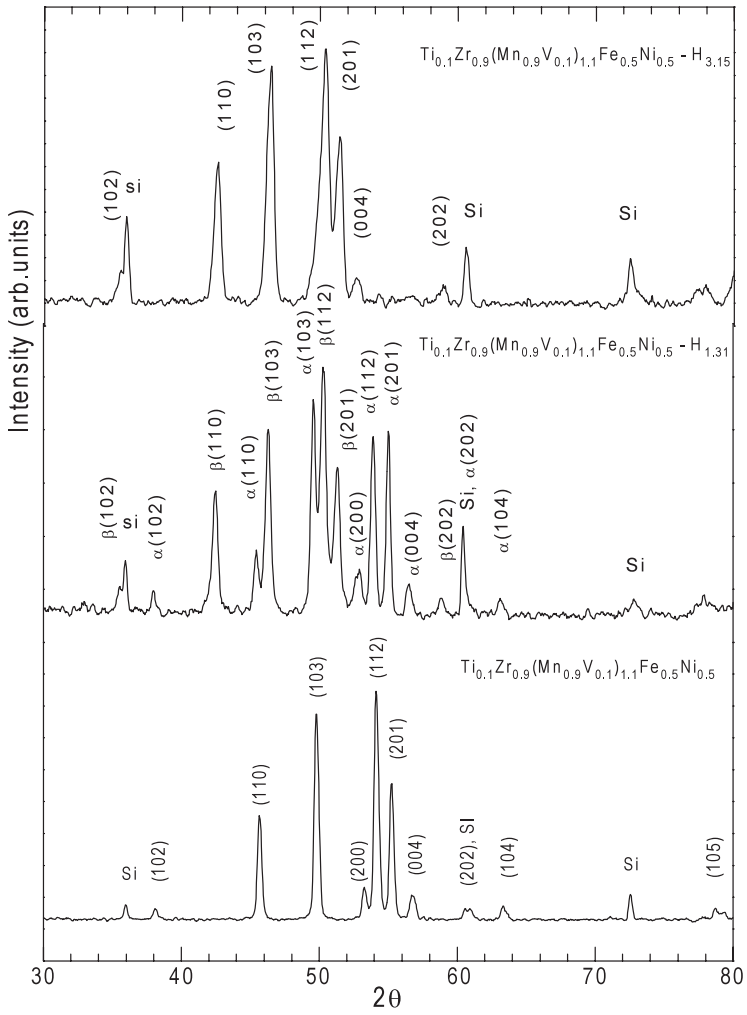

Figure 16. Powder x-ray diffractograms of $Ti_{0.1}Zr_{0.9}(Mn_{0.9}V_{0.1})_{1.1}Fe_{0.5}Ni_{0.5}$–H.

Fick's second law [24, 25]:

$$1 - \frac{m_t}{m_\infty} = \frac{6}{\pi^2}\sum_{l=1}^{\infty}\frac{1}{l^2}\exp\left(\frac{-l^2 Dt\pi^2}{r^2}\right) \tag{7}$$

for sufficiently long times; all terms except $l = 1$ can be neglected and a solution found:

$$1 - F = \begin{cases} \dfrac{6}{\pi^2}\exp\left(\dfrac{-Dt\pi^2}{r^2}\right) \\ \dfrac{6}{\pi^2}\exp(-K_{\mathrm{D}}t) \qquad K_{\mathrm{D}} = \dfrac{\pi^2 D}{r^2}. \end{cases} \tag{8}$$

By measuring the hydrogen content as a function of time (m_t) and the equilibrium hydrogen content m_α at a particular temperature, one can hence calculate the diffusion coefficient [20]. Equation (8) is of similar form to (5), and from the slope of the straight line the (β phase) diffusion coefficient has been calculated. Figure 11 shows a typical SEM image of

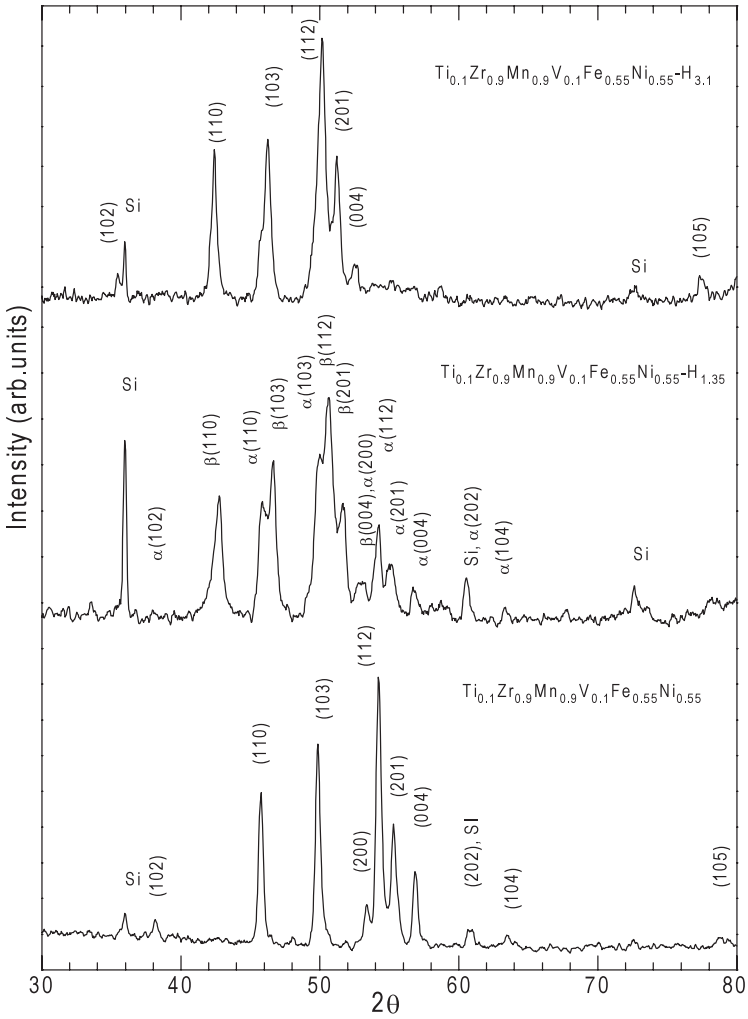

Figure 17. Powder x-ray diffractograms of $Ti_{0.1}Zr_{0.9}Mn_{0.9}V_{0.1}Fe_{0.55}Ni_{0.55}$–H.

$Ti_{0.1}Zr_{0.9}Mn_{0.9}V_{0.1}Fe_{0.5}Ni_{0.5}$ alloy hydride after several cycles of hydrogen absorption and desorption and the average particle radius is found to be 5 μm.

The diffusion coefficient thus obtained, using an average particle radius of 5 μm for $Ti_{0.1}Zr_{0.9}Mn_{0.9}V_{0.1}Fe_{0.5}Ni_{0.5}$, ranges from 2.7×10^{-11} to 1.3×10^{-10} cm^2 s^{-1} and the activation energy E_a and the corresponding frequency factor D_0 have been found to be 0.22 eV and 1.6×10^{-10} cm^2 s^{-1} respectively (figure 12).

The values of E_a in the $\alpha+\beta$ phase and β phase regions are 0.17 and 0.22 eV respectively. Hempelmann *et al* [26] have reported values of the activation energy of the order of 0.22–0.5 eV for hydrogen self-diffusion in the β phase. The values of the diffusion constant are comparable with 2×10^{-11} cm^2 s^{-1} at 30 °C for $Zr(Fe_{0.3}Mn_{0.7})_2$–H [27] and 2.2×10^{-10} cm^2 s^{-1} at 30 °C for TiFe [28] obtained by a similar procedure. The values of D obtained from the bulk measurement are three or four orders of magnitude smaller than the hydrogen diffusion coefficient of $Ti_{0.8}Zr_{0.2}CrMn$–H determined by means of neutron scattering ($D=6\times10^{-8}$ cm^2 s^{-1} at 100 K) [26].

Table 3. The lattice parameters and unit cell volume for alloys and alloy hydrides. (Note: the values of a and c (for the hydrides) are given with accuracies of 0.005 (Å) and 0.007 (Å) respectively. The value of the unit cell volume is given with an accuracy of 0.2 (Å^3).)

Sample	a (Å)	c (Å)	v (Å^3)	$\Delta v/v$ (%)
$Ti_{0.1}Zr_{0.9}Mn_{0.9}V_{0.1}Fe_{0.5}Ni_{0.5}$	4.993	8.152	176.0	—
$Ti_{0.1}Zr_{0.9}Mn_{0.9}V_{0.1}Fe_{0.5}Ni_{0.5}H_{1.4}$	5.013 (α)	8.192 (α)	178.3	1.3
	5.341 (β)	8.725 (β)	215.6	22.5
$Ti_{0.1}Zr_{0.9}Mn_{0.9}V_{0.1}Fe_{0.5}Ni_{0.5}H_{3.15}$	5.395 (β)	8.783 (β)	221.4	25.8
$(Ti_{0.1}Zr_{0.9})_{1.1}Mn_{0.9}V_{0.1}Fe_{0.5}Ni_{0.5}$	5.014	8.200	178.5	—
$(Ti_{0.1}Zr_{0.9})_{1.1}Mn_{0.9}V_{0.1}Fe_{0.5}Ni_{0.5}H_{1.5}$	5.025 (α)	8.231 (α)	180.0	0.85
	5.377 (β)	8.755 (β)	219.3	22.8
$(Ti_{0.1}Zr_{0.9})_{1.1}Mn_{0.9}V_{0.1}Fe_{0.5}Ni_{0.5}H_{3.2}$	5.379 (β)	8.766 (β)	219.7	23.1
$Ti_{0.1}Zr_{0.9}(Mn_{0.9}V_{0.1})_{1.1}Fe_{0.5}Ni_{0.5}$	5.000	8.159	176.7	—
$Ti_{0.1}Zr_{0.9}(Mn_{0.9}V_{0.1})_{1.1}Fe_{0.5}Ni_{0.5}H_{1.3}$	5.014 (α)	8.184 (α)	178.3	0.88
	5.346 (β)	8.728 (β)	216.0	22.3
$Ti_{0.1}Zr_{0.9}(Mn_{0.9}V_{0.1})_{1.1}Fe_{0.5}Ni_{0.5}H_{3.15}$	5.331 (β)	8.732 (β)	214.9	21.6
$Ti_{0.1}Zr_{0.9}Mn_{0.9}V_{0.1}Fe_{0.55}Ni_{0.55}$	4.984	8.142	175.2	—
$Ti_{0.1}Zr_{0.9}Mn_{0.9}V_{0.1}Fe_{0.55}Ni_{0.55}H_{1.35}$	4.993 (α)	8.151 (α)	176.0	0.45
	5.308 (β)	8.700 (β)	212.3	21.2
$Ti_{0.1}Zr_{0.9}Mn_{0.9}V_{0.1}Fe_{0.55}Ni_{0.55}H_{1.35}$	5.355 (β)	8.753 (β)	217.4	24.1

Figure 13 shows the kinetics of the hydrogen absorption for $Ti_{0.1}Zr_{0.9}Mn_{0.9}V_{0.1}Fe_{0.5}Ni_{0.5}$, $(Ti_{0.1}Zr_{0.9})_{1.1}Mn_{0.9}V_{0.1}Fe_{0.5}Ni_{0.5}$, $Ti_{0.1}Zr_{0.9}(Mn_{0.9}V_{0.1})_{1.1}Fe_{0.5}Ni_{0.5}$ and $Ti_{0.1}Zr_{0.9}Mn_{0.9}V_{0.1}Fe_{0.55}Ni_{0.55}$ alloys at 50 °C. It was observed that the kinetics of hydrogen absorption in $(Ti_{0.1}Zr_{0.9})_{1.1}Mn_{0.9}V_{0.1}Fe_{0.5}Ni_{0.5}$ alloy is much faster than in the other samples due to the presence of an excess amount in atomic proportion of the most reactive element Zr interacting with hydrogen.

3.4. Crystal structure of hydrides

It is known that upon hydrogenation the RCo_5 type systems will undergo structural change [29, 30]. It was observed that a hexagonal $CaCu_5$ structure changes to an orthorhombic structure upon hydrogenation in the $SmCo_5$ system. However, structural studies on $ZrMnFe_{0.5}Ni_{0.5}$ [13] show that these alloys retain the C14 hexagonal structure upon hydrogenation. X-ray powder diffraction patterns of the alloy hydrides were obtained in order to study the effect of hydrogenation on the crystal structure of the system and these are shown in figures 14–17. The powder XRD patterns show that there is no structural change upon hydrogenation and that in the mixed phase region there are two sets of Bragg reflections with each set corresponding to α and β phases. The lattice constants and unit cell volume of the hydride phase and mixed phase have been calculated using a least squares refinement technique and the calculations show a volume expansion upon hydrogenation of around 25% (table 3).

4. Conclusions

The hydrogen absorption isotherms of $Ti_{0.1}Zr_{0.9}Mn_{0.9}V_{0.1}Fe_{0.5}Ni_{0.5}$, $(Ti_{0.1}Zr_{0.9})_{1.1}Mn_{0.9}V_{0.1}Fe_{0.5}Ni_{0.5}$, $Ti_{0.1}Zr_{0.9}(Mn_{0.9}V_{0.1})_{1.1}Fe_{0.5}Ni_{0.5}$ and $Ti_{0.1}Zr_{0.9}Mn_{0.9}V_{0.1}Fe_{0.55}Ni_{0.55}$ show that the amount of hydrogen absorption is large in over-stoichiometric alloys, which can be attributed

to the increase in the atomic proportions of the hydrogen absorbing elements. At any particular temperature, the plateau pressure increases with the position of the non-stoichiometry moving from the A to the B_2 sites, which is due to the contraction of the unit cell volume. The maximum hydrogen concentration is found to be 3.5 hydrogen atoms/fu at 20 bar and 30 °C in $Ti_{0.1}Zr_{0.9}(Mn_{0.9}V_{0.1})_{1.1}Fe_{0.5}Ni_{0.5}$. The different phases present in these alloy hydrides have been identified from variations of ΔH_H with r, the kinetics of the hydrogen absorption and powder x-ray diffractograms of the alloy hydrides. The $\Delta\mu_H$ values for dissolved hydrogen in these alloy hydrides, at any particular temperature, show a linearly decreasing behaviour as the unit cell volume increases. From the kinetics of the hydrogen absorption measurements, the activation energy and the diffusion coefficient of hydrogen in $Ti_{0.1}Zr_{0.9}Mn_{0.9}V_{0.1}Fe_{0.5}Ni_{0.5}$ have been calculated to be 0.17 eV ($\alpha + \beta$ phase), 0.22 eV (β phase) and 2.7×10^{-11} cm^2 s^{-1} (β phase at 30 °C) respectively.

Acknowledgments

The authors are grateful to the MNES funding agency for supporting this work. One of the authors (MK) is grateful to IIT Madras for financial support.

References

[1] Wipf H 1997 *Hydrogen in Metals III* (*Springer Topics in Applied Physics* vol 73) (Berlin: Springer)
[2] Feng F, Geng M and Northwood D E 2000 *Int. J. Hydrog. Energy* **26** 725
[3] Van Vucht J H N, Kuijpers F A and Bruning H C A M 1970 *Philips Res. Rep.* **25** 133
[4] Reilly J J and Wiswall R H 1967 *J. Inorg. Chem.* **6** 2220
[5] Ferro R and Saccone A 1997 *Structure of Solids* (*Materials Science and Technology* vol 1) ed V Gerold (Weinheim: VCH) p 182
[6] Lee S-M, Lee H, Kim J-H, Lee P S and Lee J-Y 2000 *J. Alloys Compounds* **308** 259
[7] Kim D-M, Jang K-J and Lee J-Y 1999 *J. Alloys Compounds* **293–295** 583
[8] Anani A, Visintin A, Petrov K, Srinivasan S, Reilly J and Johnson J 1994 *J. Power Sources* **47** 261
[9] Sastri M V C, Viswanathan B and Murthy S S 1998 *Metal Hydrides, Fundamentals and Application* (New Delhi: Narosa)
[10] Kim D M, Lee S M, Jang K J and Lee J Y 1998 *J. Alloys Compounds* **268** 241
[11] Lupu D, Biris A R and Biris A S 2003 *J. Alloys Compounds* **350** 319
[12] Nakano H and Wakao S 1995 *J. Alloys Compounds* **231** 587
[13] Mani N, Sivakumar R and Ramaprabhu S 2002 *J. Alloys Compounds* **337** 148
[14] Mani N, Kesavan T R and Ramaprabhu S 2002 *J. Phys.: Condens. Matter* **14** 3939
[15] Sivakumar R 2000 *PhD Thesis* Indian Institute of Technology, Madras
[16] Xu Y-H *et al* 2001 *Int. J. Hydrog. Energy* **26** 593
[17] Flanagan T B and Park C N 1998 *Mater. Sci. Forum* **31** 297
[18] Sivakumar R, Ramaprabhu S, Rama Rao K V S, Anton H and Schmidt P C 2000 *Int. J. Hydrog. Energy* **25** 463
[19] Lee J Y, Byun S M, Park C N and Park J K 1982 *J. Less-Common Met.* **87** 149
[20] Ramesh R and Rama Rao K V S 1993 *J. Alloys Compounds* **191** 101
[21] Koh J T, Goudy A J, Huang P and Zhou G 1989 *J. Less-Common Met.* **153** 89
[22] Zarynow A, Goudy A J, Schweibenz R G and Cluy K R 1991 *J. Less-Common Met.* **172–174** 1009
[23] Wang X L and Suda S 1992 *J. Alloys Compounds* **184** 109
[24] Crank J 1956 *Mathematics of Diffusion* (Fair Lawn, NJ: Oxford University Press)
[25] Jost W 1952 *Diffusion in Solids, Liquids and Gases* (New York: Academic)
[26] Hempelmann R, Richter D, Pugliese R and Vinhas L A 1983 *J. Phys. F: Met. Phys.* **13** 59
[27] Shitikov V, Hilscher G, Stampfl H and Kirchmayr H 1984 *J. Less-Common Met.* **102** 29
[28] Lindner D L 1978 *Inorg. Chem.* **17** 3721
[29] Goudy A, Wallace W E, Craig R S and Takeshita T 1978 (Advances in Chemistry Series 167) *Thermodynamics and Kinetics of Hydrogen Absorption in Rare Earth–Cobalt and Rare Earth–Iron Compounds* ed R Bau (Washington, DC: American Chemical Society) p 312
[30] Oesterreicher H 1981 *Appl. Phys.* **24** 169